# Characterization of an inductively coupled nitrogen-argon plasma by Langmuir probe combined with optical emission spectroscopy

M. A. Song, Y. W. Lee, and T. H. Chung[a)]
*Department of Physics, Dong-A University, Busan 604-714, South Korea*

(Received 30 November 2010; accepted 23 January 2011; published online 18 February 2011)

The properties of low-pressure inductively coupled nitrogen-argon plasmas were investigated by using a Langmuir probe combined with optical emission spectroscopy (OES) under the conditions of pressures in the range of 1–30 mTorr and applied rf powers of 200–600 W. In the experiments, the argon was introduced as an actinometer and as an adding gas. The effect of the argon content in the gas mixture was examined in the range of 5%–80%. The electron energy probability function (EEPF), the electron density, and the electron temperature were obtained by using an rf-compensated Langmuir probe. The dissociation fractions were obtained from the OES actinometry. The electron temperature was also obtained by OES corona model and compared with that measured by the probe. The second positive and first negative systems of spectral bands from nitrogen molecules were analyzed to estimate the vibrational and rotational temperatures. The effects of the control parameters on the plasma parameters and dissociation fraction were investigated. While the calculated nitrogen atom density increased with power, it exhibited a maximum value near the Ar content of 30%. © *2011 American Institute of Physics*.
[doi:10.1063/1.3554706]

## I. INTRODUCTION

Nitrogen discharges in a mixture of dilution gases, such as Ar and $H_2$, as well as pure nitrogen discharges have been employed in a variety of material processing applications.[1–4] The applications include surface modification of various materials, deposition of nitride thin films, and a nitrogen atom source for the growth of semiconducting III-V nitrides by plasma assisted molecular beam epitaxy.[2] The $N_2$–Ar discharges are also applied to grow nitrides such as TiN thin films by magnetron sputtering.[3] In addition, $N_2$ plasmas with a mixture of $H_2$ were recently used to etch organic films with a low dielectric constant.[4]

Since the atomic nitrogen plays a key role in the plasma chemical processes, the concentration of atomic nitrogen in the nitrogen plasma is a significant concern.[5,6] Electric discharges produced either by microwaves, helicon waves, or rf power are commonly used for generating nitrogen atoms.[5–8] One of the promising ways to enhance the dissociation of molecular nitrogen is to introduce another gas such as hydrogen and argon in the plasma.[5] Especially, the addition of Ar to $N_2$ discharges is very useful for the easy production of stable plasmas while maintaining the significant plasma compositions over the wide range of the Ar fractions.[1,6]

Recently, there has been a steadily growing interest in inductively coupled plasma (ICP) sources for numerous plasma-enhanced materials processing because the ICP sources provide stable, reproducible, and highly uniform high density plasmas. It has been known that most $N_2$–Ar ICP discharges are characterized by high nitrogen atom content.[3] In order to characterize the $N_2$–Ar ICP discharges, the important plasma parameters that should be determined are the electron density, electron temperature, and electron energy distribution function (EEDF). Besides, both rotational and vibrational temperatures are of fundamental importance in plasma processes since the rotational excitation plays the role of a plasma thermometer whereas the vibrational excitation can trap energy and play the role of an energy reservoir, which is important for chemical reactions in plasma.[9] The convenient methods to measure these quantities include the Langmuir probe technique and optical emission spectroscopy. A clever combination of these two techniques allows us to estimate the number density of nitrogen atoms.

The dissociation fraction in an inductively coupled nitrogen plasma is important for understanding and improving the plasma processes because the number density of N atoms is deducible from the dissociation fraction. Generally, it is difficult to achieve a high dissociation efficiency of $N_2$ due to its extremely high bonding energy.[10] The dissociation of $N_2$ molecules in nitrogen plasmas has been diagnosed by using several techniques, such as mass spectrometry[2,11] and optical emission spectroscopy.[8,12–14] Nakano *et al.* measured the dissociation degree of $N_2$ in an inductively coupled plasma by using vacuum ultraviolet emission spectroscopy.[15] They observed that the dissociation fraction increased with the rf power when the $N_2$ pressure was kept at 4.98 mTorr.[15] In contrast, no large increase in the degree of $N_2$ dissociation with pressure was observed for a fixed rf power (1 kW) condition even when the electron density increased sharply in the pressure range of 0.09–4.98 mTorr.[15] Czerwiec *et al.* measured the dissociation fraction for an ICP sustained in a long cylindrical tube with a small radius specially designed for radical beam generation. They obtained a dissociation fraction from 10% (evaluated by using optical emission actinometry) up to 70% (by using mass spectrometry) for $N_2$ discharges at 50 mTorr.[2] In other works, the degree of

[a)]Electronic mail: thchung@dau.ac.kr.

 

dissociation was found to be 1%–4.9% for ICPs,[15] 0.58%–4.4% for electron-beam-excited plasmas,[10] 1%–7% for 915 MHz electron cyclotron resonance (ECR) plasmas,[5] up to 67% for high efficiency microwave plasmas,[7] 10%–40% for ICP nitrogen atom sources for molecular beam epitaxy (MBE),[8] and 1% or below for capacitive discharges.[16] The common processing reactors utilizing ICP and parallel-plate capacitive discharge have quite a low dissociation fraction. However, recent global models predict quite a high dissociation fraction of nitrogen molecules in ICP discharges.[17]

Depending on the applications, the Ar content in the mixture can vary from less than a few percent ($N_2$-dominated discharge) to over 90% (Ar-dominated discharge). The gas pressure is also dependent on the application and the size of the ICP chamber and rf antenna. In order to meet the demand of the process, the plasma properties should be clarified for different gas pressure, Ar content, and rf power and be tailored for specific applications. The optical emission actinometry has only a limited use in plasmas in which the content of the actinometer gas (Ar in this work) is less than a few percent (e.g., 3% or less). As will be seen later, the use of actinometry can be extended to the region of a higher Ar content although it gives a rough estimation of the neutral density (N in this work).

The purpose of this work is to characterize the properties of inductively coupled $N_2$–Ar discharges with varying operating parameters. The operating parameters, such as the Ar content in the gas mixture, applied rf power, and total gas pressure, have been varied in an attempt to fully characterize plasma parameters and nitrogen atom production. The electron temperature is obtained by analyzing the optical emission spectra from excited Ar atoms and then comparing with the values given by the Langmuir probe at different powers (200–600 W) in the pressure range 1–30 mTorr, which is different from the range of similar studies.[10,15,16] Also, the vibrational and rotational temperatures of nitrogen molecules are obtained. The density of a neutral nitrogen atom is estimated by using optical emission actinometry. The dependence of nitrogen atom density on the control parameters is explored and some physical explanations are given with a discussion of the plasma properties such as the electron density, the electron temperature, and the electron energy distribution function measured by a Langmuir probe.

## II. EXPERIMENT

A schematic diagram of the experimental setup with the diagnostics system [optical emission spectroscopy (OES) and Langmuir probe] is shown in Fig. 1. The plasma chamber consists of a stainless-steel cylinder with a 28 cm diameter and a 34 cm length. A 1.9-cm-thick by 27-cm-diameter tempered glass plate mounted on one end separates the planar one-turn induction coil from the plasma. The induction coil is made of copper (with water-cooling) and is connected to an L-type capacitive matching network and a rf power generator.

The plasma chamber is evacuated by using a diffusion pump backed by rotary pump giving a base pressure of $5\times10^{-6}$ Torr. The equilibrium gas pressure in the chamber

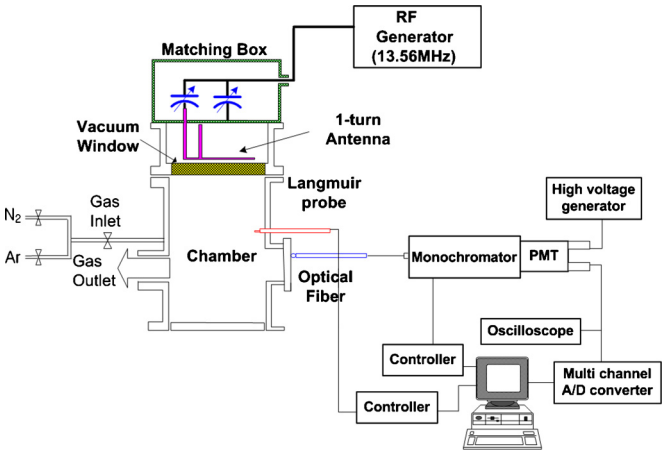


FIG. 1. (Color online) Schematic diagram of experimental setup and diagnostics system.

is monitored with a combination vacuum gauge (IMG 300). The operating gas pressure is controlled by adjusting the mass flow controller. The nitrogen gas pressure is varied in the range of 1–30 mTorr, and a 13.56 MHz generator (ENI OEM 12) drives a rf current in a flat one-turn coil through the rf power generator and matching network. The source gas is $N_2$ gas. The argon is introduced as an actinometer and as an adding gas. The Ar content in the gas mixture is varied in the range of 5%–80%.

Light collection was made by an optical fiber (0.1 mm slit diameter) attached to the $CaF_2$ window. The light intensity of emissive molecules and radicals in the plasma was focused by means of an optical fiber into the entrance slit of 0.75 m monochromator (SPEX 1702) equipped with a grating of 1200 grooves per millimeter and a slit width of 100 $\mu$m. The light was collimated at the exit slit where a photomultiplier tube converted photons into an electric signal. Optical emission spectra were recorded in the wavelength range of 250–850 nm with a resolution of 0.1 nm. The measured emission spectra should be corrected for the spectral response of the detection system, which includes optical fiber, monochromator, and photomultiplier tube. The detection system had to be calibrated in intensity using a quartz halogen lamp with a known spectral radiance. In plasma processing, the most useful and well developed technique to determine the density of neutral species is actinometry. In this method, a known concentration of an impurity is introduced and the intensities of two neighboring spectral lines, one from the known gas and one from the sample, are compared. Since both species are bombarded by the same electron distribution and the concentration of the actinometer is known, the density of the sample can be calculated.

An rf-compensated cylindrical single Langmuir probe is mounted through one of the ports on the vacuum chamber. The probe tip, made of tungsten with a diameter of 0.1 mm and a length of 10 mm, is used to measure the plasma parameters. The probe tip is located on the axis of the cylinder 14 cm below the tempered glass plate. To measure the plasma parameters, the harmonic technique, which exploits the generation of harmonics resulting from the excitation of

the nonlinearity of the single Langmuir probe characteristics, combined with the Druyvesteyn method was used. In the harmonic method,[18] the voltage applied to the probe consists of the sweep voltage and the sinusoidal voltage of the frequency $\omega$. The second harmonic term $I_{2\omega}$ of the measured probe current is proportional to the second derivative, $d^2I/dV^2$, which is related to the electron energy distribution function (EEDF), $f(\epsilon)$. The electron density $(n_e)$ and the effective electron temperature $(T_e)$ are calculated with the measured EEDF as follows.

$$n_e = \int_0^{\epsilon_{max}} f(\epsilon)d\epsilon, \quad T_e = \frac{2}{3n_e}\int_0^{\epsilon_{max}} \epsilon f(\epsilon)d\epsilon, \tag{1}$$

where $\epsilon_{max}$ is determined by the dynamic range of the EEDF measurement. The electron temperature can also be determined from the slope of the probe I-V curve in the exponential region (from the point where the probe current is zero to where the slope of the curve begins to decrease). We observe that both methods yield almost same values of the electron temperature.

## III. DETERMINATION OF PLASMA TEMPERATURES AND ACTINOMETRY MODEL

Low-pressure glow discharges are nonequilibrium plasmas with the temperature of electrons higher than the neutral gas temperature. Molecular gases can also be characterized by vibrational $(T_{vib})$ and rotational $(T_{rot})$ temperatures. For low-pressure $N_2$–Ar plasmas, direct excitation from the ground state with radiative decay can be assumed to dominate over the production and destruction of excited energy levels. For instance, many excited states of argon are mainly produced by electron-impact excitation from the ground state,[19] and the quenching rate of excited nitrogen and argon atoms by both $N_2$ molecules and Ar atoms is very small compared to the radiative decay.[12] This simplification is called the corona balance. Gordillo-Vázquez *et al.*[19] investigated the corona model and obtained a modified Boltzmann formula as follows.

$$\ln\left(\frac{I_{ij}\lambda_{ij}\Sigma_{i>j}A_{ij}}{A_{ij}a_{1i}}\right) = -\frac{E_i}{k_BT_e} + const, \tag{2}$$

where $I_{ij}$ and $\lambda_{ij}$ are, respectively, the intensity and wavelength of spectral lines, $A_{ij}$ is the Einstein coefficient, $E_i$ is the excitation energy of level $i$, $k_B$ is the Boltzmann constant, and $a_{1i}$ is the coefficient in an exponential approximation of the electron-impact excitation rate coefficient from ground state to level $i$.

Generally, the line intensity of the radiative transition of a molecule can be expressed as[20]

$$I(n',v',J' \rightarrow n'',v'',J'') = h\nu A(n',v',J' \rightarrow n'',v'',J'')N_{n',v',J'}, \tag{3}$$

where $I(n',v',J' \rightarrow n'',v'',J'')$ is the intensity of the spectrum ($n$ is the electronic state, $v$ is the vibrational quantum number, and $J$ is the rotational quantum number), $h$ is Planck's constant, $\nu$ is the frequency of the radiative transition, $A(n',v',J' \rightarrow n'',v'',J'')$ is the transition probability, and $N_{n',v',J'}$ is the number density of the molecules in the upper states.

When we assume a Boltzmann distribution for the vibrational and rotational states, $N_{n',v',J'}$ is rewritten as

$$N_{n',v',J'} = N_{n'}\, exp(-E_{vib}/k_BT_{vib})(2J'+1) \times exp(-E_{rot}/k_BT_{rot}) \tag{4}$$

where $N_{n'}$ is a constant independent of $v$ and $J$, $T_{vib}$ and $T_{rot}$ are the vibrational and rotational temperatures, respectively, and $E_{vib}$ and $E_{rot}$ are the vibrational and rotational energy levels, respectively. In this study, we analyzed the second positive system of a nitrogen molecule to estimate the vibrational and rotational temperatures. Considering the above equations, we can determine these temperatures by fitting the calculated spectrum with that measured experimentally. In order to evaluate the gas temperature in the discharge, the evolution of the $N_2^+$ first negative emission system is also monitored. $N_2$ molecules exchange rotational and translational energy faster with Ar atoms than with electrons and, as a consequence, the rotational distribution quickly achieves thermodynamic equilibrium with Ar gas. Therefore, a convenient way to determine the gas temperature is through the measurement of the rovibrational band spectrum of nitrogen.[21]

A kinetic analysis of $N_2$–Ar discharge under the assumption of quasistatic equilibrium gives

$$[N^*] = \frac{n_e[N]k_N^{dir} + n_e[N^m]k_{N^m}^{exc} + n_e[N_2]k_{N_2}^{diss-exc} + [Ar^*][N]k_N^{Penn} + [Ar^*][N_2]k_N^{Penn-diss}}{\frac{1}{\tau_N} + k_{N^*}^{Q}[Ar]}, \tag{5}$$

where [N], [N*], and [N$^m$] are the population densities of the ground state N(2p $^4$S), the excited state N*(3p $^4$S), and the metastable states [N$^m$(2p $^2$D) and N$^m$(2p $^2$P)] of species N, respectively. The $k_N^{dir}$ is the rate coefficient for electronic excitation of the ground state, $k_{N^m}^{exc}$ is the rate coefficient for electronic excitation of the metastable state, $k_{N_2}^{diss-exc}$ is the

rate coefficient for electronic dissociative excitation of molecule $N_2$, $k_N^{Penn}$ is the rate coefficient for Penning excitation of the ground state N due to the excited states of Ar, $k_N^{Penn-diss}$ is the rate coefficient for Penning dissociation of $N_2$ due to the excited states of Ar, $\tau_N$ is the lifetime of the excited state, and $k_{N^*}^Q$ is the rate coefficient for quenching by argon. Usually, at low-pressure discharges, $k_{N^*}^Q[\mathrm{Ar}]$ is much less than $1/\tau_N$, thus the quenching term can be neglected.

The emission intensity due to a transition from an excited level $[N^*(3p\ ^4S)]$ to a lower state $[N^*(3s\ ^4P)]$ is

$$I(\mathrm{N}^*) = K_N h \nu_N A_N [\mathrm{N}^*], \tag{6}$$

where $K_N$ is a factor depending on the plasma volume, solid angle, and spectral response of the spectrometer, $\nu_N$ is the frequency of the transition, and $A_N$ is the optical emission probability for the transition. When $k_{N^*}^Q$ is ignored, Eq. (6) can be expressed as

$$I(\mathrm{N}^*) = K_N h \nu_N A_N \tau_N n_e [\mathrm{N}] k_N^{dir} (1 + s_1), \tag{7}$$

where $s_1$ is the correction factor accounting for various contributions to the formation of excited nitrogen atoms rather than the direct excitation by electron impact. If we assume that the excited state of Ar participating in Penning reaction is only Ar metastable, from Eqs. (5)–(7), we have

$$s_1 = \frac{n_e[\mathrm{N^m}]k_{N^m}^{exc} + n_e[\mathrm{N_2}]k_{N_2}^{diss-exc} + [\mathrm{Ar^m}][\mathrm{N}]k_N^{Penn} + [\mathrm{Ar^m}][\mathrm{N_2}]k_N^{Penn-diss}}{n_e[\mathrm{N}]k_N^{dir}}. \tag{8}$$

The rate coefficients $k_{N^m}^{exc}, k_{N_2}^{diss-exc}, k_N^{Penn}, k_N^{Penn-diss}$ are less than $k_N^{dir}$ by one order of magnitude.[2,22] Unless the densities of metastable N and Ar atoms are large, the factor $s_1$ is very small.

Similarly, the emission intensity from an excited Ar atom is written as

$$I(\mathrm{Ar}^*) = K_{Ar} h \nu_{Ar} A_{Ar} \tau_{Ar} n_e [\mathrm{Ar}] k_{Ar}^{dir} (1 + s_2), \tag{9}$$

where $s_2$ is the correction factor accounting for the excitation from the metastable Ar,

$$s_2 = \frac{[\mathrm{Ar^m}]k_{Ar^m}^{exc}}{[\mathrm{Ar}]k_{Ar}^{dir}}. \tag{10}$$

For the optical emission actinometry utilizing a $N_2$–Ar gas mixture, the emission of the N line at 746.68 nm $(3p\ ^4S_{3/2} \rightarrow 3s\ ^4P_{5/2})$ is selected and the Ar line at 750.4 nm $(2p_1 \rightarrow 1s_2$ transition) is used because it is not sensitive to two step excitation.

From Eqs. (7) and (9),

$$\frac{[\mathrm{N}]}{[\mathrm{Ar}]} = \frac{I_{746}}{I_{750}} \frac{(1+s_2)}{(1+s_1)} \frac{K_{750}}{K_{746}} \frac{\nu_{750}}{\nu_{746}} \frac{A_{750}}{A_{746}} \frac{k_{Ar}^{dir}}{k_N^{dir}} \frac{\tau_{750}}{\tau_{746}}. \tag{11}$$

If the measured spectral response $K_{750}=0.0158$ and $K_{746}=0.0185$ and values of $A$ and $\tau$ from the literature[2,12] are used, the nitrogen atom density is derived as

$$[\mathrm{N}] = 1.61 \frac{I_{746}}{I_{750}} \frac{(1+s_2)}{(1+s_1)} \frac{k_{Ar}^{dir}}{k_N^{dir}} \frac{x_{Ar}}{x_{N_2}} [\mathrm{N_2}], \tag{12}$$

where $x_{Ar}$, $x_{N_2}$, and $[N_2]$ are the percentages of argon and nitrogen in the gas mixture with the discharge off and the input number density of nitrogen molecules, respectively. However, quantitatively accurate results can only be obtained if excitations via dissociative channels, Penning effect, and the quenching of excited states are accounted for.

In reality, the experimental determination of $[N^m]$ and $[Ar^m]$ is difficult and the data set for the reaction coefficients involved in Eq. (8) are insufficient. Therefore, the evaluation of the correction factors with varying Ar content is a formidable task. As will be seen, with varying Ar content, the $s_1$ factor does not exhibit a big change because both $[N^m]$ and $[Ar^m]$ are countervariant quantities (both [N] and $[N_2]$ also). The $s_2$ factor increases with the Ar content but the effect of $s_2$ is also not significant due to small values of $[Ar^m]$. Therefore the actinometric relation, Eq. (12), can be used to give a rough estimation of [N] even for the high Ar content discharges. A recent study by Kimura *et al.*[1] indicates that a simple actinometry without the correction factors results in a considerable agreement with the global model considering the full set of chemical reactions.

In this work, we obtain the dissociation fraction (thus, the nitrogen atom density) for an inductively coupled $N_2$–Ar discharge as functions of Ar content. In order to better understand the effects of these parameters on the dissociation fraction, we utilize electron energy probability function (EEPF) and the electron density and electron temperature that were measured by using the Langmuir probe.

## IV. RESULTS AND DISCUSSION

Figure 2(a) shows the electron energy probability functions (EEPFs) for different Ar contents at the power of 500 W and pressure of 1.4 mTorr. The EEPFs were observed to be Maxwellian in a rough manner. The Ar-dominating plasma is Maxwellian and noise-free. Low-energy and high-energy electron groups occur as in most radio-frequency discharges.[23] For most of the mixture plasmas, the population of electrons with energies greater than 12 eV exhibits an unstable behavior, which might be caused by noise. Also, the

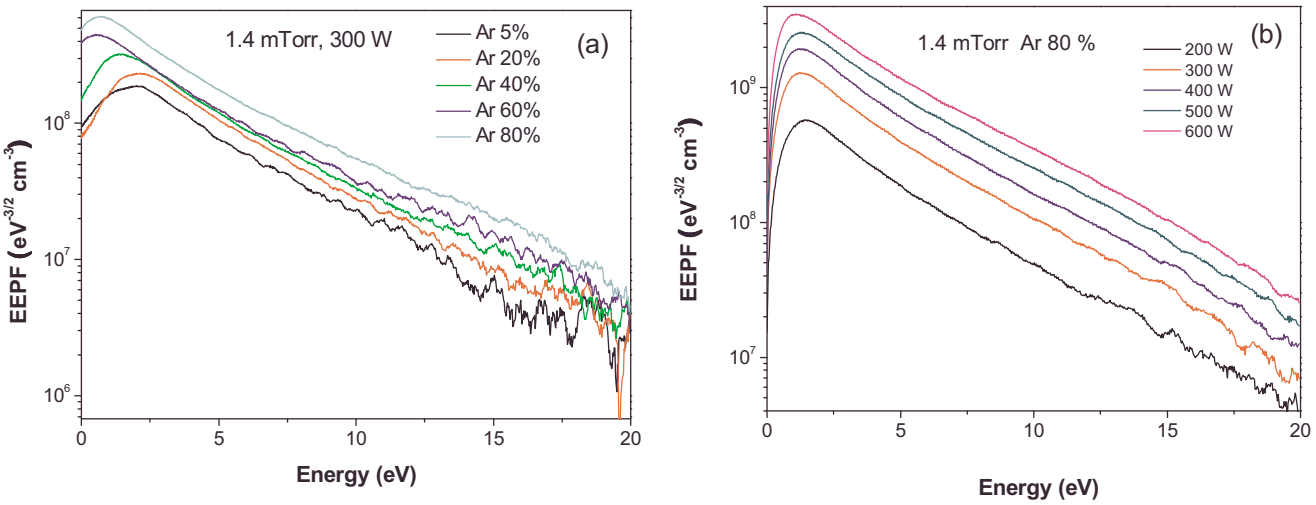


FIG. 2. (Color online) (a) Electron energy probability functions (EEPFs) for different Ar contents at the power of 500 W and the pressure of 1.4 mTorr. (b) EEPFs for different powers at 1.4 mTorr for Ar 80% discharges.

easy heating due to frequent electron-impact rovibrational excitations of nitrogen molecules is thought to contribute to the fluctuation of the probe currents. For nitrogen, the threshold for dissociation is at 9.8 eV; however, the cross section function does not rise significantly until after 15 eV. From there, it rises gradually to a value of $6.74\times10^{-17}$ cm$^2$ at 20 eV.[16] Generally, very little $N_2$ is dissociated because of the high threshold and the peak energy well above 20 eV. However, ICP discharges show a considerable amount of high-energy electron, and this may promote the dissociation of $N_2$. Figure 2(b) shows the EEPFs for different powers at the pressure of 1.4 mTorr. The EEPFs show that the electron density increases with power and Ar content. The number of electrons having an energy above 15 eV was observed to increase with the Ar content and with increasing power. These electrons contribute to an increase in the electron-impact dissociation.

Figure 3 shows the electron density and the electron temperature obtained by a Langmuir probe measurement as functions of power and Ar content. The electron density increases with pressure. With an increase in the Ar content, the electron density increases and the electron temperature slightly decreases. This can be explained by a spatially averaged model of particle and power balance in $N_2-Ar$ discharge.[1,17] The particle balance equation is written as

$$(k_{iz}^{N_2}n_e[N_2]+k_{iz}^{N}n_e[N]+k_{iz}^{Ar}n_e[Ar])V = (2\pi R^2h_l+2\pi RLh_R)n_eu_B, \tag{13}$$

where $R$, $L$, and $V$ are the radius, the height, and the volume of the cylindrical chamber, respectively. Here, $k_{iz}^{N_2}$, $k_{iz}^{N}$, and $k_{iz}^{Ar}$ denote the rate coefficients of the electron-impact ionization of $N_2$, N, and Ar, respectively, and $u_B$ is the Bohm velocity. The factors $h_l$ and $h_R$ are the edge to center positive ion density ratios in the axial and radial direction given as[24]

$$h_l=\frac{0.86}{\sqrt{3+\frac{L}{2\lambda_i}}},\quad h_R=\frac{0.8}{\sqrt{4+\frac{R}{\lambda_i}}}, \tag{14}$$

where $\lambda_i$ is the ion mean free path in $N_2-Ar$ plasma given by

$$\frac{1}{\lambda_i}=[Ar]\sigma_{Ar}+[N_2]\sigma_{N_2}+[N]\sigma_N, \tag{15}$$

where $\sigma_{Ar},\sigma_{N_2},\sigma_N$ are the total ion-neutral collision cross sections.

Rearranging Eq. (13), we have

$$k_{iz}^{N_2}[N_2]+k_{iz}^{N}[N]+k_{iz}^{Ar}[Ar]=\frac{u_B}{d_{eff}}, \tag{16}$$

where $d_{eff}$ is the effective length $[=RL/2(Rh_l+Lh_R)]$. It should be noted that as the Ar content increases, $\lambda_i$ is decreased. This causes the $h_l$ and $h_R$ factors to decrease, thus making $d_{eff}$ increase, which results in a slight decrease in $T_e$.

The power balance equation for electrons is given by

$$P_{abs}=e\varepsilon_c^{N_2}k_{iz}^{N_2}n_e[N_2]V+e\varepsilon_c^{N}k_{iz}^{N}n_e[N]V+e\varepsilon_c^{Ar}k_{iz}^{Ar}n_e[Ar]V + e(\varepsilon_e+\varepsilon_i)n_eu_BA_{eff}, \tag{17}$$

where $P_{abs}$ is the net power absorbed in the plasma and $A_{eff}(=V/d_{eff})$ is the effective area of the chamber. The collisional energy loss per electron-ion pair created $\varepsilon_c$ represents the power loss due to elastic and inelastic collisions, which includes all excitation energies such as vibrational, dissociative, and electronic excitations. Here, $\varepsilon_c^{N_2}$ and $\varepsilon_c^{N}$ are the collisional energy loss per ionization event of nitrogen molecule and nitrogen atom, respectively, and $\varepsilon_c^{Ar}$ is the collisional electron energy loss per ionization event of argon gas. The average energy of escaping ions, $\varepsilon_i$, is the sum of the ion energy entering the sheath $(T_e/2)$ and the energy gained in the sheath $V_{sh}$ (sheath voltage drop), and $\varepsilon_e$ is the average energy of electrons escaping to the walls and is assumed to be equal to 2 $T_e$. Combining Eqs. (16) and (17), we have

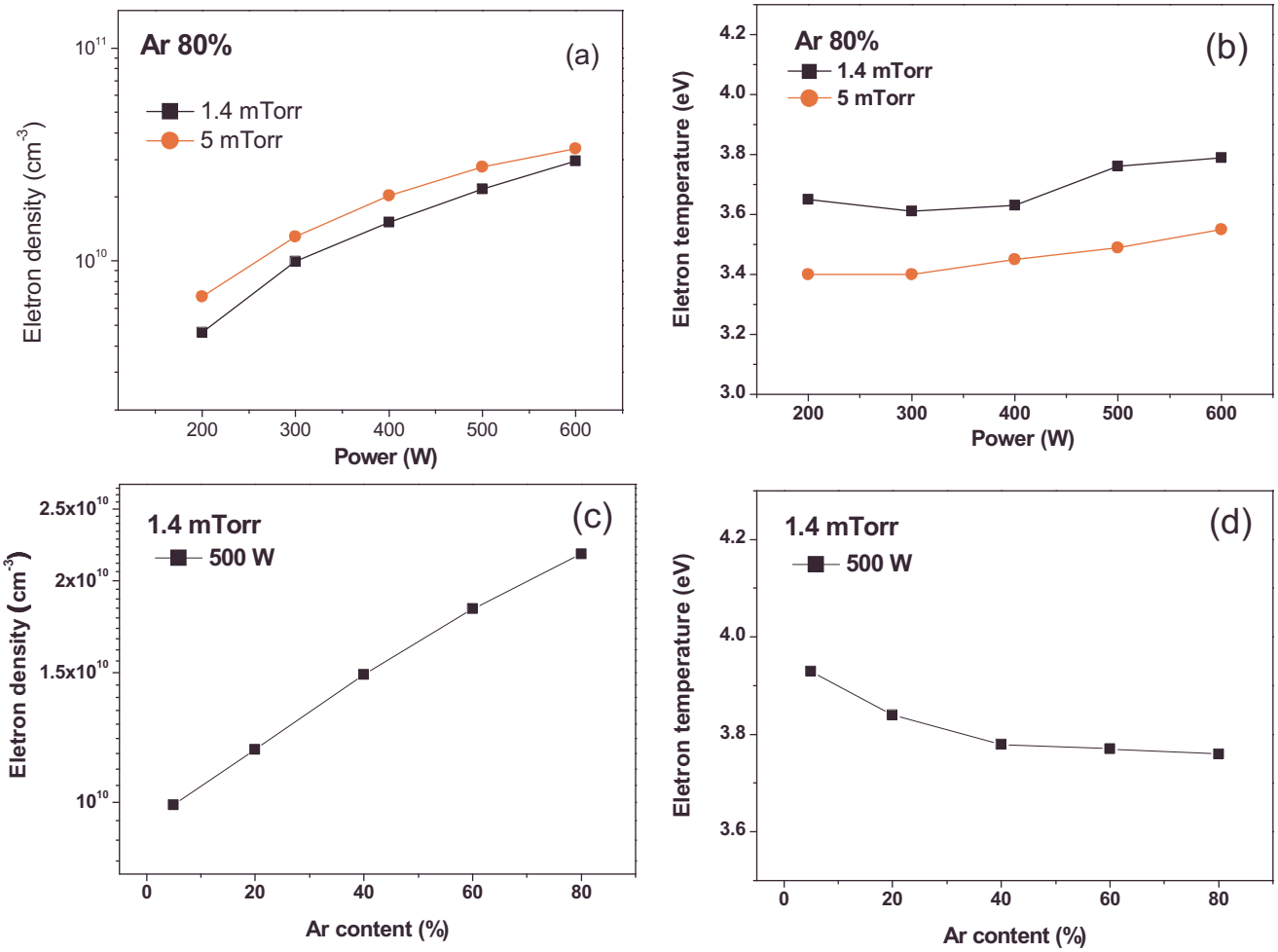


FIG. 3. (Color online) (a) Electron density and (b) electron temperature obtained by using a Langmuir probe as functions of power for 1.4 mTorr and Ar 80%. (c) Electron density and (d) electron temperature as a function of the Ar content for 1.4 mTorr and 500 W.

$$n_e = \frac{P_{abs}}{eu_B A_{eff}(\varepsilon_c^{N_2}\delta_{N_2} + \varepsilon_c^{N}\delta_{N} + \varepsilon_c^{Ar}\delta_{Ar} + \varepsilon_e + \varepsilon_i)}, \quad (18)$$

where $\delta_{N_2}=n_{N_2^+}/n_e$, $\delta_N=n_{N^+}/n_e$, $\delta_{Ar}=n_{Ar^+}/n_e$. As the Ar content increases, the term $\varepsilon_c^{N_2}\delta_{N_2}+\varepsilon_c^{N}\delta_N+\varepsilon_c^{Ar}\delta_{Ar}$ decreases because $\varepsilon_c^{N_2}$ and $\varepsilon_c^{N}$ are several times larger than $\varepsilon_c^{Ar}$ at $T_e=3-5$ eV.[17] Therefore, $n_e$ increases with the Ar content in the operating region of this work. As usual, the electron temperature decreases with pressure and increases slightly with power. This trend is in agreement with the modeling and the experimental work.[25] The electron density and electron temperature are then used to evaluate the dissociation fraction of $N_2$.

Figure 4(a) presents a typical optical emission spectrum of ICP nitrogen-argon plasmas operated in 1.4 mTorr at the applied power of 600 W. The main emission peaks correspond to several transition lines of atomic nitrogen, argon atom, and molecular nitrogen. The spectrum is characterized by the $N_2$ first positive band system (FPS) $[B\ ^3\Pi_g(v') \rightarrow A\ ^3\Sigma_u^+(v'')]$, the $N_2$ second positive band system (SPS) $[C\ ^3\Pi_u(v') \rightarrow B\ ^3\Pi_g(v'')]$, and the $N_2^+$ first negative band system (FNS) $[B\ ^2\Sigma_u^+(v') \rightarrow X\ ^2\Sigma_g^+(v'')]$. Here, $v'$ and $v''$ are the vibrational quantum numbers of the upper and lower states. The spectra are dominated by strong molecular features, which peak around 300–400 nm and 600–800 nm. The most dominant peak of the first negative system is at 391.4 nm (0,0). The first positive system covers in a wavelength range of 600–800 nm. The most intense emission intensities from $N_2$ second positive system [337.1 nm (0,0), 315.9 nm (1,0), and 357.7 nm (0,1)], etc., are caused by many excitation and quenching processes such as the electron-impact excitation from the ground state and the excitation from the first metastable state $N_2(A\ ^3\Sigma_u^+)$ due to collision with metastable state $Ar^m$, which indicates the overpopulation of $N_2(C\ ^3\Pi_u)$.[15,26] Therefore, it is observed that the most intense peak of the second positive system is large compared with the peak of the $N_2$ first positive system and $N_2^+$ first negative system. The reason for this phenomenon is the energy pooling reaction caused by the effective lifetime of the first metastable state $N_2(A\ ^3\Sigma_u^+)$, which has the lowest threshold energy (6.2 eV) and a long lifetime (about 2 s).[27] The insets show the emission lines at 537.3 and 687.1 nm. Since these two lines are very weak in general, the observation of these lines with a reasonable signal-to-noise ratio makes the optical measurement more convincing.

The relative spectral response of the detection system employed in this work is as follows: 0.479 (337.1 nm), 0.448 (391.4 nm), 0.0185 (746.8 nm), 0.0158 (750.4 nm), and

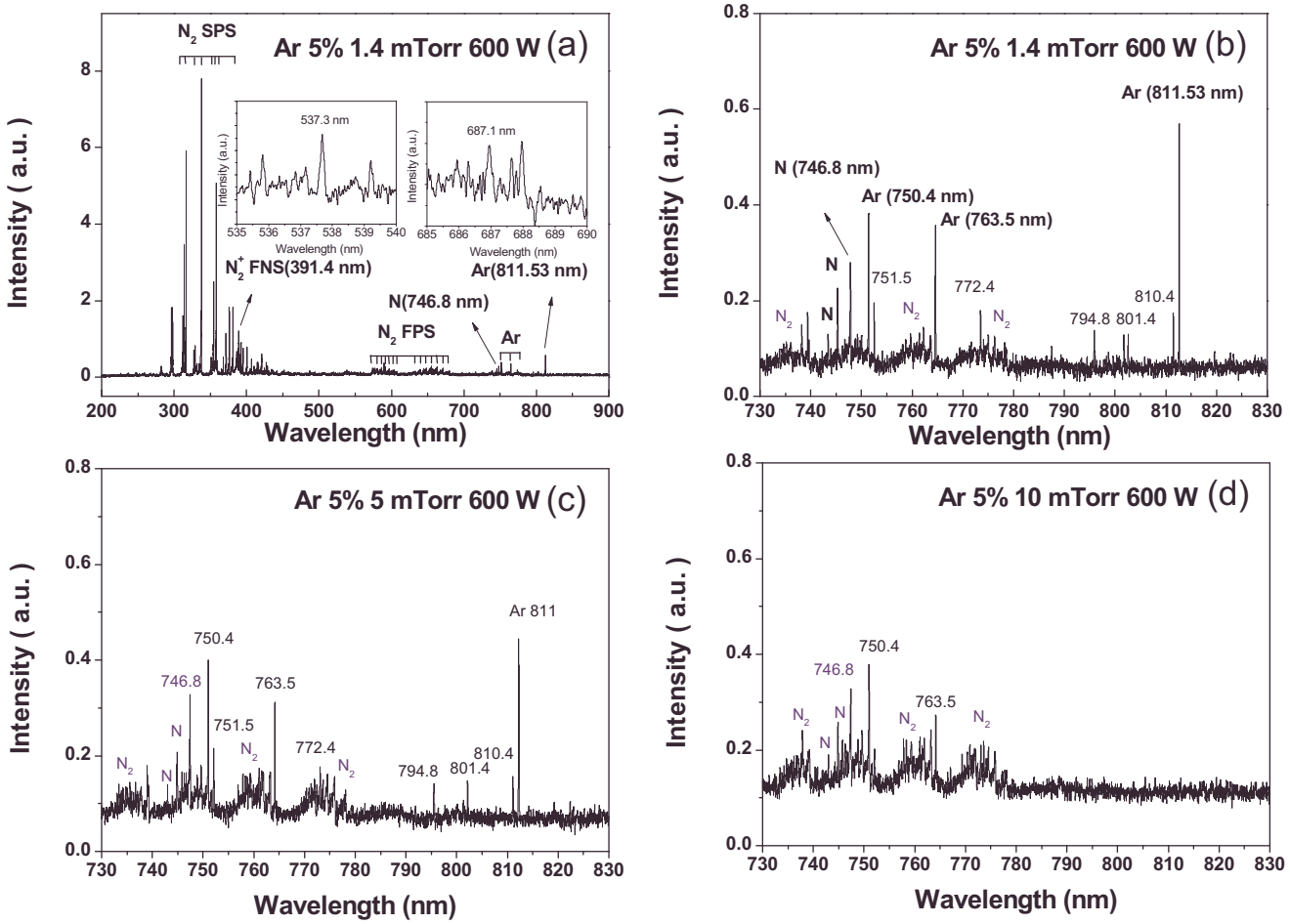


FIG. 4. (Color online) (a) Spectrum of optical emission from inductively coupled nitrogen discharge at $p=1.4$ mTorr and $P=600$ W. The insets represent the emission lines at 537.3 and 687.1 nm. Feed gas compositions are 5% Ar and 95% $N_2$. The spectra with a range of 730–830 nm at (b) $p=1.4$ mTorr, (c) $p=5$ mTorr, and (d) $p=10$ mTorr.

0.0068 (811.5 nm). Although the intensities of peaks with wavelengths above 600 nm seem small, the concentrations of the excited states of those species are not actually small. As expected, the emission intensities of all peaks were observed to increase with increasing power.

Figure 4(b) shows the same spectrum with a narrow range of wavelength (730–830 nm). There exist many Ar peaks at 750.4 nm ($2p_1 \rightarrow 1s_2$), 811.5 nm ($2p_9 \rightarrow 1s_5$), 763.5 nm ($2p_6 \rightarrow 1s_5$), 772.4 nm ($2p_2 \rightarrow 1s_3$), 794.8 nm ($2p_4 \rightarrow 1s_3$), 810.4 nm ($2p_7 \rightarrow 1s_4$), and 801.4 nm ($2p_8 \rightarrow 1s_5$). In addition, the N peaks appear at 746.8 nm ($3p\ ^4S \rightarrow 3s\ ^4P_{5/2}$), 744.2 nm ($3p\ ^4S \rightarrow 3s\ ^4P_{3/2}$), and 742.3 nm ($3p\ ^4S \rightarrow 3s\ ^4P_{1/2}$). As shown in Figs. 4(b)–4(d), as the pressure increases, the overall intensities of these lines decrease. The optical spectrum from the 5 mTorr discharge shows an insignificant change compared to that of the 1.4 mTorr discharge. However, when the gas pressure increases to 10 mTorr, the argon peaks except 750.4 and 763.5 nm are almost smeared out. This can be explained by the fact that the $2p \rightarrow 1s$ transitions are suppressed since the excitation of the ground state Ar to 2p levels is diminished due to the decrease of the electron temperature with increasing pressure. Although not shown in the figure, the intensities from SPS at 5 mTorr increased compared to those at 1.4 mTorr but decreased at 10 mTorr. In addition, at 10 mTorr, the most intense peak is at 357.7 nm (0,1) rather than 337.1 nm (0,0), indicating that the vibrational energy distribution of the nitrogen molecules depends on the pressure.

As can be seen from Fig. 4, an increase in the Ar content made a noticeable influence on the emission spectrum. As expected, the intensities of the Ar peaks increase but the intensities of the typical lines of the $N_2$ first and second positive systems and $N_2^+$ first negative system were slightly decreased. By decreasing the supply of molecular $N_2$ with an increase of the Ar content, the populations of the excited N, $N_2$, and $N_2^+$ would also decrease. However, with an increase of Ar content, the Penning excitation and Penning dissociation due to $Ar^m$ increase the densities of the excited states of N, $N_2$, and $N_2^+$, trading off the decrease in the supply of $N_2$. An increase in the Ar content results in a slight increase of the emission intensity from N atoms.

Figure 5(a) shows the modified Boltzmann plot obtained from Ar lines for Ar 80% plasma at 500 W and 1.4 mTorr. The electron temperature found by linear fitting of the high-energy Ar peaks (537.3, 687.1, 696.5, 706.8, 714.7, and 750.4 nm) is about 3.14 eV. When the pressure is 22 mTorr, $T_e$ is decreased to 1.26 eV. Figure 5(c) presents $T_e$ obtained

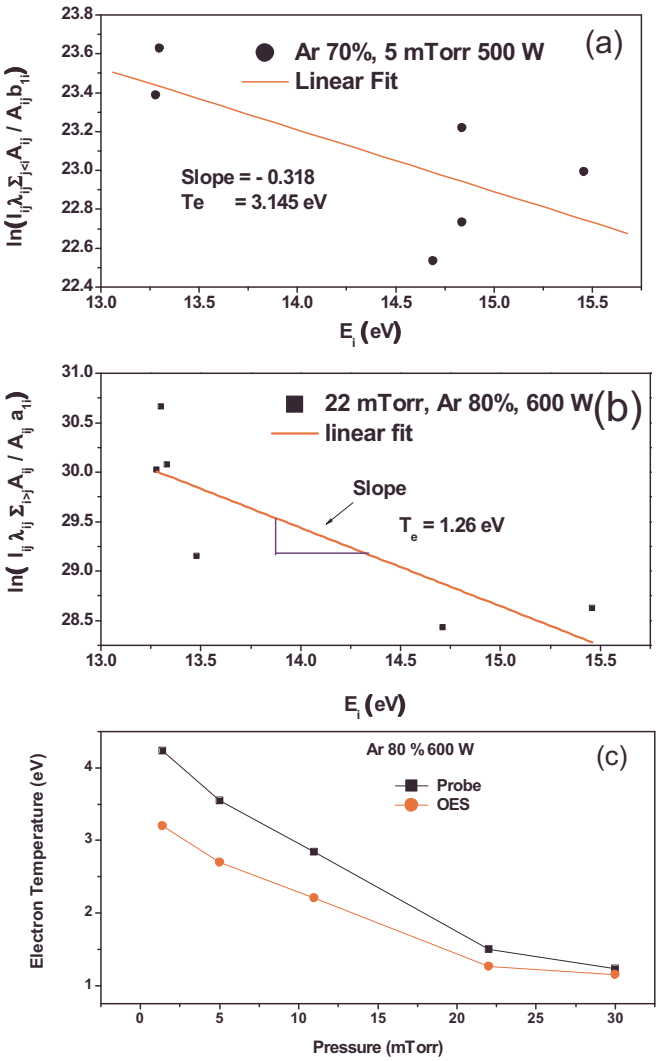


FIG. 5. (Color online) The modified Boltzmann plot obtained from Ar lines for (a) 1.4 mTorr and (b) 22 mTorr of the Ar 80% plasma at 500 W. The $T_e$ value deduced from linear fit is indicated. $E_i$ is the energy of the upper levels of the radiative transition. (c) Comparison of the electron temperatures as a function of pressure measured by the OES and by the Langmuir probe.

by a Langmuir probe and spectroscopic measurements. The values of the electron temperature measured by the OES based on the corona balance of Ar excited atoms are a little lower than those obtained by a Langmuir probe. This can be explained by the fact that the Langmuir probe is more accurate for low-energy electrons while the OES techniques are more sensitive to high-energy electrons. Considering the uncertainties on spectroscopic measurements, the values in both cases give a very good agreement and so this result corroborates the reliability of data obtained with both techniques.

Figure 6(a) represents the spectrum of the second positive system of the $N_2$ $[C\ ^3\Pi_u(v') \rightarrow B\ ^3\Pi_g(v'')]$ and first negative system of $N_2^+$ in the spectral range of 300–400 nm. An example of a generated rovibrational spectrum for the $\Delta v = -4$ and $-3$ band sequence in the first positive system of $N_2$ is shown in Fig. 6(b). A method of rotational and vibrational temperature estimation in nitrogen plasma by simulation of the emission spectrum of the first positive system $B\ ^3\Pi_g(v') \rightarrow A\ ^3\Sigma_u^+(v'')$ of nitrogen was also introduced by Biloui *et al.*[28]

For vibrational transitions, the transition probability is written as[28]

$$A(v' \rightarrow v'') = \frac{64\pi^4}{3h\lambda^3} q_{v',v''} R_e^2, \tag{19}$$

where $\lambda$, $q_{v',v''}$, and $R_e$ are the wavelength of the radiative transition, the Franck–Condon factor, and the electronic-vibrational transition moment, respectively. In Fig. 7(a), the Boltzmann plot method was applied to the emission intensity peaks relating to $\Delta v = -1$ of the second positive system to estimate the vibrational temperature. The inset represents the normalized distribution of the vibrational state. The $T_{vib}$ value deduced from linear fit is indicated. When the discharge parameters are Ar 80%, $p = 5$ mTorr, and $P = 400$ W, the $T_{vib}$ value was 15 100 K. Figure 7(b) shows the vibrational temperature of $N_2(C)$ as a function of the Ar content for different gas pressures. The vibrational temperature increases with the Ar content and decreases with pressure. The measured vibrational temperature compares well with those from the previous works.[9,29] It should be noted that each electronic state of $N_2$ (ground state X and excited states A, B, and C) has different vibrational distributions.[30] Hence, each state has different vibrational temperatures. The vibrational temperature estimated from the emission spectrum of the first positive system $B\ ^3\Pi_g(v') \rightarrow A\ ^3\Sigma_u^+(v'')$ of nitrogen molecule corresponds to the $T_{vib}$ of $N_2(B)$. However, its trend of change with control parameters is expected to be similar. It is known that the vibrational temperature is related to vibrational excited particle density $N_v$; the increase of vibrational temperature indicates an increase in the relative population $R(=N_v/N_0)$ of vibrational excited particles, which are generated by electron impact expressed by $N_v = k_v n_e N_0$, where $N_0$ is the $v = 0$ particle density of a specific electronic state and $k_v$ is the vibrational excitation rate coefficient.[31] From this equation, the relative population of the vibrational excitation particles is proportional to both $n_e$ and the vibrational excitation rate coefficient $k_v$, while $k_v$ depends strongly on the electron temperature in the plasma. With the increase of the discharge pressure, the collision rate between molecules increases and makes the collisional relaxation of molecules proceed more rapidly. Therefore, the $N_2$ vibrational temperature decreases with increasing pressure. This trend was also observed in a dual-frequency capacitive discharge.[31]

To estimate the rotational temperatures of plasmas, the simulated spectra of the $N_2^+$ first negative system band transition of nitrogen $[B\ ^2\Sigma_u^+(0) \rightarrow X\ ^2\Sigma_g^+(0)]$ are compared to the measured spectra.[32,33] The rotational temperatures are obtained when the best fits are achieved. A typical fitting of the measured first negative (0,0) band spectrum with the synthetic spectrum is shown in Fig. 8(a). A good agreement between the measured spectrum and the synthetic suggests a reasonable evaluation of $T_{rot}$. In Fig. 8(b), the $N_2$ rotational temperature-based estimation of neutral temperature is plotted as the Ar content. The $T_{rot}$ increases with the Ar content. This can be explained by the fact that a higher population of

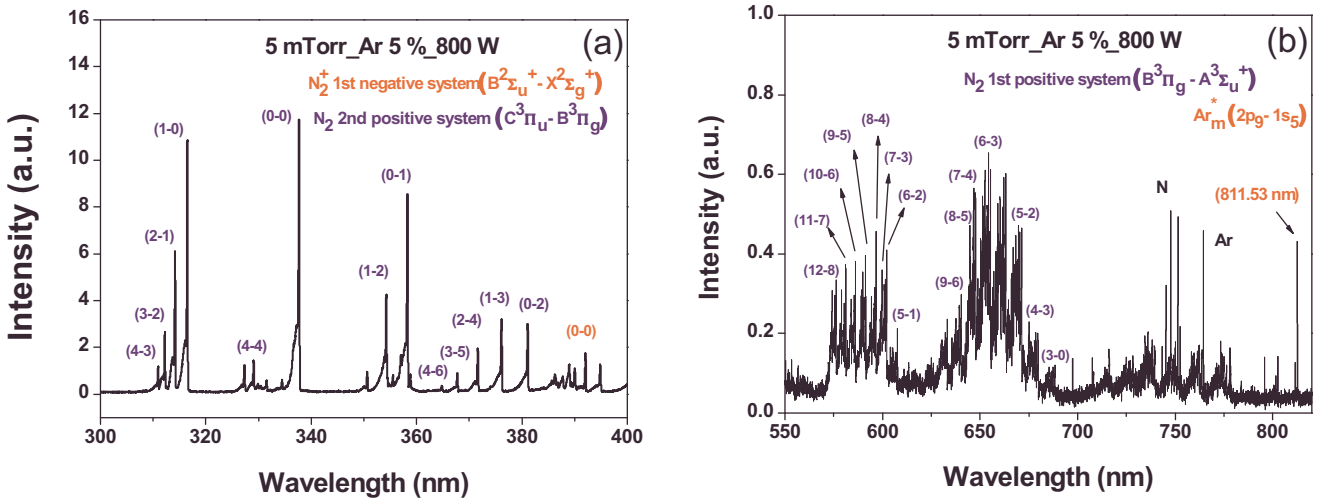


FIG. 6. (Color online) (a) Spectra of optical emission from the second positive system of $N_2$ [$C\ ^3\Pi_u(v') \rightarrow B\ ^3\Pi_g(v'')$] and the first negative system of $N_2^+$ in the spectral range of 300–400 nm at $p=5$ mTorr and $P=600$ W. (b) Experimental spectrum of the $\Delta v=-4$ and $-3$ band sequence in the first positive system of $N_2$.

$Ar^m$ leads to a frequent excitation to higher rotational energy levels in $N_2(C,v')$ since they have comparable energies.

Using Eq. (3), the rotational and vibrational temperatures of plasmas can be estimated simultaneously.[34] In Fig. 8(c), the simulated and measured spectra of the $N_2$ second positive system transition are compared in the spectral range of 300–360 nm. The curves were intentionally shifted vertically for better separation. Two spectra (one is intentionally shifted vertically) are for the same rotational and vibrational temperatures. When the discharge parameters are Ar 5%, $p=5$ mTorr, and $P=600$ W, $T_{rot}$ and $T_{vib}$ were 400 and 9163 K, respectively. This method gives the results in good agreement with those shown in Fig. 7(b). The rotational temperatures can be measured using various transition bands from $N_2(C,v')$, $N_2(B,v')$, and $N_2^+(B,v')$. It is found out that all these transitions result in comparable values of $T_{rot}$. Although these may be different from the rotational temperature of the ground state $N_2(X,v')$, these can represent the rotational temperature of nitrogen molecules also being equal to the gas temperature.

In Fig. 9(a), the intensity ratios, $I_{746.8}/I_{750.4}$, as a function of power are presented for different Ar contents at the pressure of 1.4 mTorr. Based on Eq. (12) without the correction factors, the dissociation fraction can be calculated as: 0.0385 (Ar 5%), 0.166 (Ar 20%), 0.236 (Ar 40%), and 0.523 (Ar 80%). The intensity ratios increase slightly with power. Noting that $T_e$ is observed to increase with power (in Fig. 3) and the ratio $k_{Ar}^{dir}/k_N^{dir}$ in Eq. (12) increases with $T_e$, the dissociation fraction increases with power.

In nitrogen plasmas, the atomic nitrogen species are mainly produced by electron-impact processes such as the dissociative collisions between electrons and nitrogen molecules or between electrons and nitrogen molecular ions (dissociative recombination).[5] These processes strongly depend

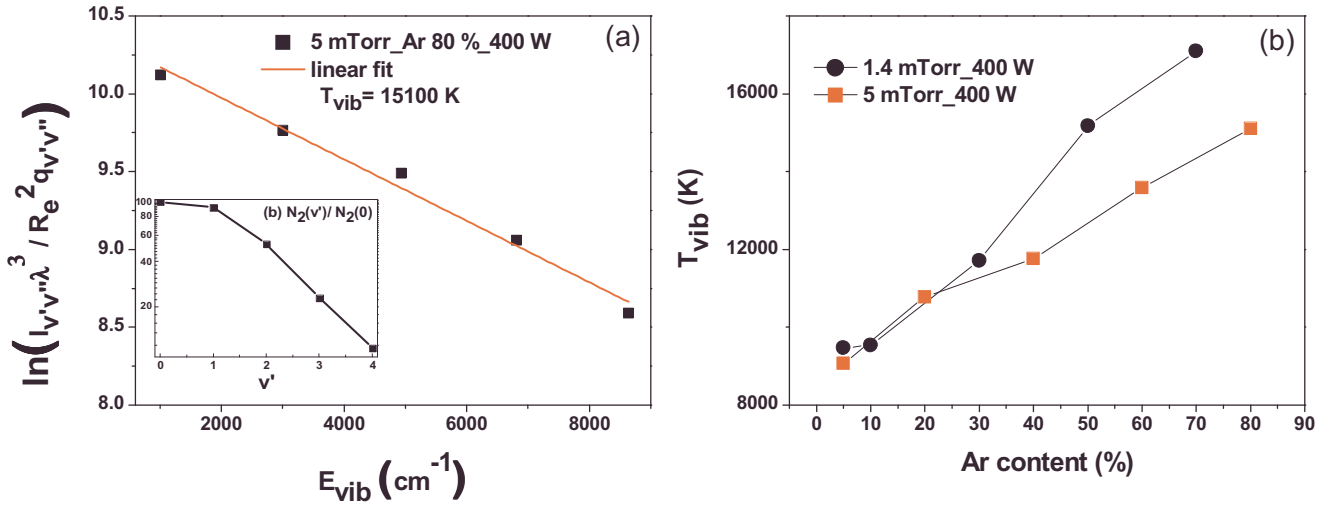


FIG. 7. (Color online) (a) The Boltzmann plot of the emission intensity peaks relating to $\Delta v=-1$ of the second positive system of $N_2$. The inset represents the normalized distribution of the vibrational state. Discharge parameters: Ar 5%, $p=5$ mTorr, and $P=400$ W. (b) Vibrational temperatures as a function of the Ar content for different pressures.

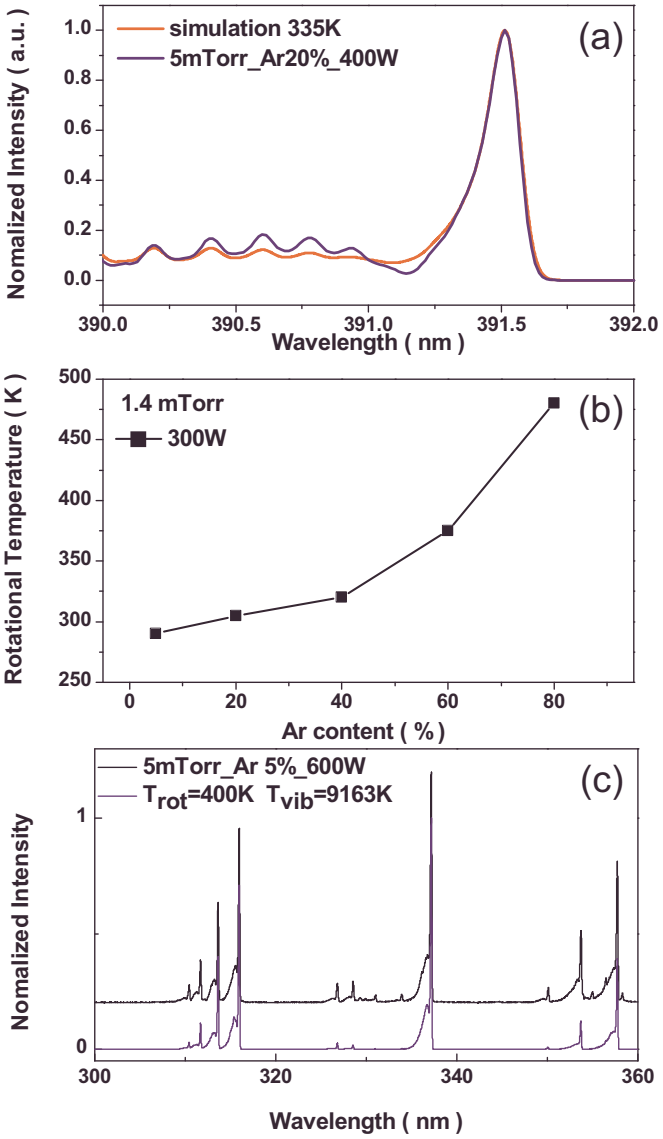


FIG. 8. (Color online) (a) A typical fitting of the measured first negative (0, 0) band spectrum of the first negative system of $N_2^+$ with the synthetic spectrum. (b) Rotational temperatures as a function of the Ar content. (c) Simulated and measured spectra of $N_2$ second positive system transition are compared in the spectral range of 300–360 nm. One curve is shifted vertically for better separation. Two spectra are for the same rotational and vibrational temperatures.

on the electron temperature. However, in nitrogen-argon plasmas, there exists a dissociation mechanism associated with the excited state Ar. That is the reason why the correction factors in Eq. (12) should be considered.

The density of the N-metastable, $[N^m(^2D)]$, is about 0.1–0.3 times the density of the ground state species and $[N^m(^2P)]$ is smaller than $[N^m(^2D)]$ by one order of magnitude.[16,17] The excitation rate coefficient $k_{N^m}^{exc}$ is less than $k_N^{dir}$ by a factor of 10 at $T_e$=4–5 eV.[2] Therefore, the excitation from $N^m(^2D)$ to $N^*(3p\ ^4S)$ is small. However, introducing Ar into the nitrogen plasma causes the generation of $N_2(B)$, $N_2(C)$, $N_2^+(X)$, and $N_2^+(B)$.[32] The interaction of these with the ground state nitrogen atoms may result in the enhancement of $[N^m]$. However, the change of $[N^m]$ with the Ar content will not be considered in the analysis of this study. The dissociative excitation rate coefficient $k_{N_2}^{diss-exc}$ is less than $k_N^{dir}$ by a factor of 1000 at $T_e$=4–5 eV.[2] The factor $s_1$ is written as

$$s_1 \approx 0.1\frac{[N^m]}{[N]} + 0.001\frac{[N_2]}{[N]} + \frac{[Ar^m][N_2]k_N^{Penn-diss}}{n_e[N]k_N^{dir}}. \quad (20)$$

The values of $k_N^{Penn} \simeq k_N^{Penn-diss} = 3\times10^{-11}$ and $k_N^{dir} = 8\times10^{-10}$ cm$^3$/s at $T_e$=5 eV are used. The value of $[Ar^m]$ can be estimated from the intensity ratio of Ar 750.4 nm to 811.5 nm and the rate coefficients $k_{Ar^m}^{exc}$ and $k_{Ar}^{dir}$.[35] At $p$=1.4 mTorr, the values of $[Ar^m]/[Ar]$ were found as: 0.10% (Ar 5%), 0.28% (Ar 20%), 0.56% (Ar 40%), 0.94% (Ar 60%), and 1.20% (Ar 80%). Utilizing the obtained values of $[N]/[N_2]$ (without correction) and assuming $[N^m]/[N] \approx 0.1$, we can estimate the correction factors: $s_1$ are 0.263 (Ar 5%), 0.503(Ar 20%), 1.002 (Ar 40%), 1.063 (Ar 60%), and 1.098 (Ar 80%), and $s_2$ are 0.006 (Ar 5%), 0.0168 (Ar 20%), 0.0336 (Ar 40%), 0.0564 (Ar 60%), and 0.072 (Ar 80%). In this calculation, the neutral particle densities are obtained using the relation $[N_2]=px_{N_2}/k_BT_{rot}$.

With the correction factors estimated, the nitrogen atom density can finally be calculated using Eq. (12). The values of the electron-impact excitation cross sections are obtained from the literature.[22] In deriving the rate coefficient, a Maxwell–Boltzmann energy distribution of electrons was used. Figure 9(b) is the plot of the calculated nitrogen atom densities as a function of the Ar content. As can be seen, the nitrogen atom density reaches a maximum at the Ar content of 30% and decreases afterwards. It should be noted that the Ar 30% discharge has a much higher nitrogen atom density than that of the Ar 5% discharge. A proper mixing of Ar gas to nitrogen gas proved to promote dissociation. As shown in Fig. 9(a), the dissociation fraction ($[N]/[N_2]$) increased with both increasing power and Ar content, which is in agreement with a global model.[17]

Discharges with a higher Ar content result in a higher dissociation fraction. This is related to the increase in the density of Ar metastables because the relative production of Ar metastables increases with the Ar content. The Ar metastables $1s_5$ and $1s_3$ are at energy levels of 11.55 and 11.72 eV, respectively.[16] These metastables have significant interactions with nitrogen molecules through a resonant energy transfer called the Penning excitation. The excited nitrogen molecules can dissociate to form two nitrogen atoms. The Ar metastable density was found to be between ~0.1% (Ar 5%) and ~1.2% (Ar 80%) of the ground state density, which is well compared to the literatures.[3,16] There is also another contribution to N-atom production: The charge exchange between nitrogen molecules and argon ions followed by dissociative recombination.[2]

To explore the dependence of dissociation on $n_e$ and $T_e$, a simple scaling relation can be utilized. Neutral nitrogen atoms are assumed to be generated mainly by the electron-impact dissociation of $N_2$ (and partly by the Penning dissociation due to the excited Ar), and to be lost by diffusion to and recombination at the reactor wall and by the electron-impact ionization of N. Then we have

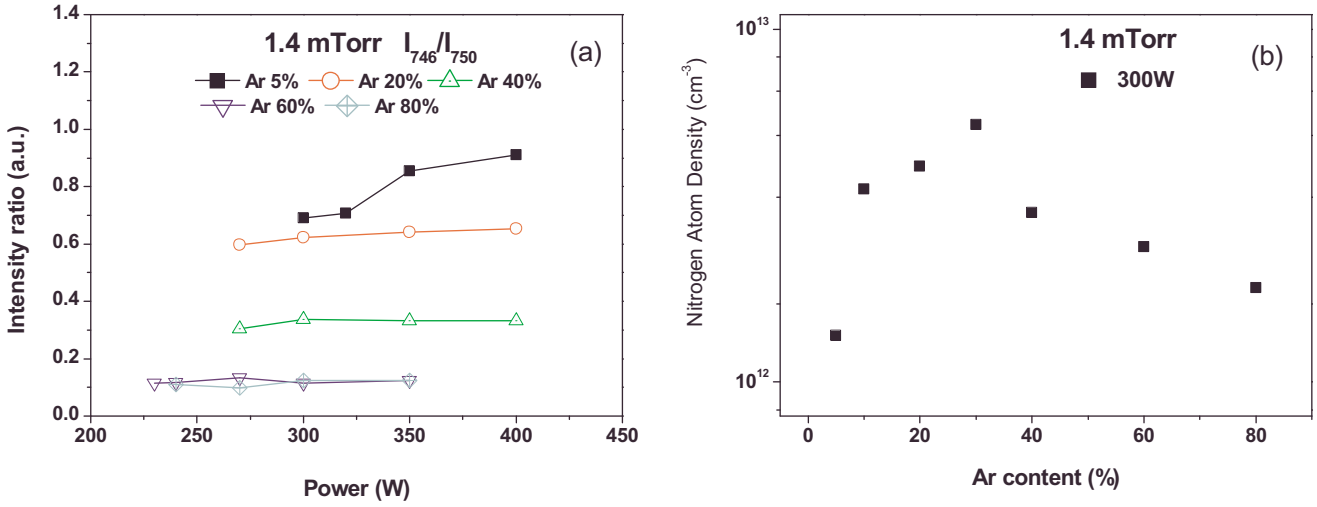


FIG. 9. (Color online) (a) Intensity ratio $I_{746.8}/I_{750.4}$ as a function of power for different Ar contents at the pressure of 1.4 mTorr. (b) Calculated nitrogen atom densities as a function of the Ar content.

$$2K_{diss}n_e[\mathrm{N_2}] + k_N^{Penn-diss}[\mathrm{Ar^*}][\mathrm{N_2}] \approx (K_d + k_{iz}^N n_e)[\mathrm{N}], \tag{21}$$

where $K_{diss}$ is the rate coefficient for dissociation of $N_2$ and $K_d$ is the rate coefficient for the diffusion to and recombination at the reactor wall of N atoms. Assuming that metastable Ar plays an important role, the nitrogen atom density is approximated by

$$[\mathrm{N}] \approx \frac{2K_{diss}n_e + k_N^{Penn-diss}[\mathrm{Ar^m}]}{K_d + k_{iz}^N n_e}[\mathrm{N_2}]. \tag{22}$$

If $K_{diss}$ and $k_{iz}^N$ are assumed to have Arrhenius forms $K_{diss}=K_{diss0}e^{-\varepsilon_{diss}/T_e}$, $k_{iz}^N=k_{iz0}e^{-\varepsilon_{iz}/T_e}$ [$\varepsilon_{diss}$ (=9.8 eV) and $\varepsilon_{iz}$ (=14.5 eV) are the threshold energies for dissociation and ionization reactions],[36] then $K_{diss}$ and $k_{iz}^N$ decrease with decreasing electron temperature ($k_{iz}^N$ has a steeper variation). It is worth noting that if we look into the electron energy dependence of the cross section of nitrogen dissociation, $\varepsilon_{diss}$ should be replaced by the real activation energy, which is a little higher than the threshold energy (but lower than $\varepsilon_{iz}$).

In Fig. 3, it is observed that $T_e$ decreases and $n_e$ increases as the Ar content is increased. The electron-impact reaction rates show an exponential dependence on $T_e$ and generally exhibit linear variations in $n_e$. The $k_{iz}^N n_e$ decreases dominantly over $K_{diss}n_e$ with a decrease in $T_e$ (indicated as $\Downarrow$ below). The increase in the Ar content decreases the recombination at the walls due to a decreased flux of N atoms to the wall, resulting from a lower amount of $N_2$ in the chamber and the increased flux of the Ar ions to the walls.[16] Therefore, with an increase of the Ar content, we have a simple scaling

$$[\mathrm{Ar}]\uparrow,[\mathrm{N_2}]\downarrow,n_e\uparrow,T_e\downarrow,K_d\downarrow,k_{iz}^N\Downarrow,K_{diss}\downarrow,[\mathrm{Ar^m}]\uparrow,[\mathrm{N}]\nearrow\searrow. \tag{23}$$

Until the Ar content of 30%, a decrease in the denominator of Eq. (16) dominates (and $[Ar^m]$ increases) over a slight decrease of the numerator due to the value of $[N_2]$, then the [N] increases. Afterwards, the numerator also decreases because the increase rate of $[Ar^m]$ with Ar content is lower than the decrease rate of $[N_2]$; therefore, [N] decreases. Although not shown in the figures, the dissociation fraction was observed to decrease slightly with pressure at a higher pressure region than 10 mTorr. This can be accounted for by the fact that the wall recombination increased. As the power is increased, the dissociation fraction is observed to increase. From the global balance of the discharge kinetics, the dissociated neutral atom density is expected to be proportional to the power.[36] The trend of change in the dissociation fraction correlates well with the electron density and the electron energy probability function.

It seems that the OES actinometry provides quite large values of the dissociation fraction for low-pressure inductively coupled $N_2$–Ar discharges. In low-temperature nitrogen plasmas, the main neutral constituent is $N_2$. Therefore, the dissociative excitation process must be also be considered since it often yields a very important contribution.[37] The actinometry for discharges with larger contents of Ar would give an overestimated value for dissociation fraction because the Penning excitation of nitrogen atoms due to excited Ar and/or dissociative excitation of nitrogen molecules due to Ar metastables should be considered. The correction factors can be determined more accurately with advanced diagnostics methods such as laser induced fluorescence or laser absorption spectroscopy.[38] Then the nitrogen atom density can be measured more precisely.

## V. CONCLUSION

The diagnostics of low-pressure inductively coupled $N_2$–Ar plasmas by using OES and Langmuir probe were performed under the conditions of gas pressures in the range of 1.4–30 mTorr and applied powers in the range of 200–600 W. Increases in power resulted in the increase of the overall intensity of the optical emission spectrum. It was observed that the addition of Ar increased the dissociation fraction of $N_2$. With the Ar content increased, the Penning excitation of N and the Penning dissociation of $N_2$ due to Ar metastables

increased. With increasing Ar content, the electron density was found to increase and the electron temperature slightly decreased. The population of the electrons in the high-energy region of the EEPF is also responsible for the enhancement of the dissociation fraction. The values of the electron temperature measured by the OES based on the corona balance of Ar excited atoms were well compared with those obtained by a Langmuir probe. The rotational and vibrational temperatures of $N_2^+$ and $N_2$ were calculated based on the $N_2^+$ first negative system $B\ ^2\Sigma_u^+(v') \rightarrow X\ ^2\Sigma_g^+(v'')$ and $N_2$ second positive system $C\ ^3\Pi_u(v') \rightarrow B\ ^3\Pi_g(v'')$ from the molecular optical emission spectrum in the wavelength from 300 to 400 nm. The method of a point to point comparison of an experimental measured spectrum with a simulated one by a least-square procedure was used in this work. The changes of the rotational and vibrational temperatures with the Ar content as well as the gas pressure were discussed. The dissociation fraction increased with increasing power, as expected. We have shown that increasing the Ar content causes significant changes in the properties of discharge such as gas temperature, rovibrational excitation, EEDF, and dissociation fraction. A higher Ar content caused an enhancement of the dissociation fraction. At the pressure of 1.4 mTorr, the nitrogen atom density had a maximum value near the Ar content of 30%. These findings may lead to a better understanding of plasma chemistry that maximize dissociation of feed gases.

## ACKNOWLEDGMENTS

This research was supported by the Basic Science Research Program through the National Research Foundation of Korea (NRF) funded by the Ministry of Education, Science, and Technology (Grant No. 2009-0070839).

[1] T. Kimura and H. Kasugai, J. Appl. Phys. **108**, 033305 (2010).
[2] T. Czerwiec, F. Greer, and D. B. Graves, J. Phys. D **38**, 4278 (2005).
[3] K. Tao, D. Mao, and J. Hopwood, J. Appl. Phys. **91**, 4040 (2002).
[4] K. Ishikawa, Y. Yamaoka, M. Nakamura, Y. Yamazaki, S. Yamasaki, Y. Ishikawa, and S. Samukawa, J. Appl. Phys. **99**, 083305 (2006).
[5] N. Itagaki, S. Iwata, K. Muta, A. Yonesu, S. Kawakami, N. Ishii, and Y. Kawai, Thin Solid Films **435**, 259 (2003).
[6] W.-Y. Ding, J. Xu, W.-Q. Lu, X.-L. Deng, and C. Dong, Phys. Plasmas **16**, 053502 (2009).
[7] R. W. McCullough, J. Geddes, J. A. Croucher, J. M. Woolsey, D. P. Higgins, M. Schlapp, and H. B. Gilbody, J. Vac. Sci. Technol. A **14**, 152 (1996).
[8] D. Voulot, R. W. McCullough, W. R. Thompson, D. Burns, J. Geddes, Q. J. Gosimini, E. Nelson, P. P. Chow, and J. Klaassen, J. Vac. Sci. Technol. A **16**, 3434 (1998).
[9] N. Britun, M. Gaillard, A. Ricard, Y. M. Kim, and J. G. Han, J. Phys. D **40**, 1022 (2007).
[10] S. Tada, S. Takashima, M. Ito, M. Hori, T. Goto, and Y. Sakamoto, J. Appl. Phys. **88**, 1756 (2000).
[11] D. Douai, J. Berndt, and J. Winter, Plasma Sources Sci. Technol. **11**, 60 (2002).
[12] V. Henriques, E. Tatarova, F. M. Dias, and C. M. Ferreira, J. Appl. Phys. **91**, 5632 (2002).
[13] Y. Wang, R. J. Van Brunt, and J. K. Olthoff, J. Appl. Phys. **83**, 703 (1998).
[14] Y. M. Shin, E. Y. Kim, and T. H. Chung, J. Korean Phys. Soc. **53**, 617 (2008).
[15] T. Nakano, S. Kumagai, and S. Samukawa, J. Appl. Phys. **92**, 2990 (2002).
[16] M. A. Worsley, S. F. Bent, N. C. M. Fuller, and T. Dalton, J. Appl. Phys. **100**, 083301 (2006).
[17] E. G. Thorsteinsson and J. T. Gudmundsson, Plasma Sources Sci. Technol. **18**, 045001 (2009).
[18] J. Y. Bang, A. Kim, and C. W. Chung, Phys. Plasmas **17**, 064502 (2010).
[19] F. J. Gordillo-Vázquez, M. Camero, and C. Gómez-Aleixandre, Plasma Sources Sci. Technol. **15**, 42 (2006).
[20] T. Sakamoto, H. Matsuura, and H. Akatsuka, J. Appl. Phys. **101**, 023307 (2007).
[21] C. Foissac, C. Dupret, and P. Supiot, J. Phys. D **42**, 015206 (2009).
[22] R. M. Frost, P. Awakowicz, H. P. Summers, and N. R. Badnell, J. Appl. Phys. **84**, 2989 (1998).
[23] J. Pulpytel, W. Morscheidt, and F. Arefi-Khonsari, J. Appl. Phys. **101**, 073308 (2007).
[24] V. A. Godyak, *Soviet Radio Frequency Discharge Research* (Delphic, Falls Church, VA, 1986).
[25] J. Ma and Y. K. Pu, Phys. Plasmas **10**, 4118 (2003).
[26] S. Agarwal, B. Hoex, M. C. M van de Sanden, D. Maroudas, and E. S. Aydil, Appl. Phys. Lett. **83**, 4918 (2003).
[27] N. K. Bibinov, A. A. Fateev, and K. Wiesemann, J. Phys. D **34**, 1819 (2001).
[28] C. Biloiu, X. Sun, Z. Harvey, and E. Scime, Rev. Sci. Instrum. **77**, 10F117 (2006).
[29] E. J. Tonnis and D. B. Graves, J. Vac. Sci. Technol. A **20**, 1787 (2002).
[30] V. Guerra, P. A. Sa, and J. Loureiro, Eur. Phys. J.: Appl. Phys. **28**, 125 (2004).
[31] X.-J. Huang, Y. Xin, L. Yang, Q.-H. Yuan, and Z.-Y. Ning, Phys. Plasmas **15**, 113504 (2008).
[32] V. Linss, H. Kupfer, S. Peter, and F. Richter, J. Phys. D **37**, 1935 (2004).
[33] S. Y. Moon and W. Choe, Spectrochim. Acta, Part B **58**, 249 (2003).
[34] X. Lu, Q. Xiong, Z. Xiong, J. Hu, F. Zhou, W. Gong, Y. Xian, C. Zou, Z. Tang, Z. Jiang, and Y. Pan, J. Appl. Phys. **105**, 043304 (2009).
[35] G. A. Piech, J. B. Boffard, M. F. Gehrke, L. W. Anderson, and C. C. Lin, Phys. Rev. Lett. **81**, 309 (1998).
[36] M. A. Lieberman and A. J. Lichtenberg, *Principles of Plasma Discharge and Materials Processing* (Wiley, New York, 1994), p. 487.
[37] M. Abdel-Rahman, V. Schulz-von der Gathen, T. Gans, K. Niemi, and H. F. Dobele, Plasma Sources Sci. Technol. **15**, 620 (2006).
[38] Y. Hayashi, S. Hirao, Y. Zhang, T. Gans, D. O'Connell, Z. Lj. Petrovic, and T. Makabe, J. Phys. D **42**, 145206 (2009).